Journal of Computational Physics 371 (2018) 712–731

Contents lists available at ScienceDirect

Journal of Computational Physics

www.elsevier.com/locate/jcp

An integral equation approach to calculate electrostatic interactions in many-body dielectric systems

Eric B. Lindgren [a,b], Anthony J. Stace [c], Etienne Polack [d], Yvon Maday [d,e,f], Benjamin Stamm [b,*], Elena Besley [c,*]

[a] Aachen Institute for Advanced Study in Computational Engineering Science (AICES), RWTH Aachen University, Schinkelstr. 2, 52062 Aachen, Germany
[b] Center for Computational Engineering, Mathematics Department, RWTH Aachen University, Schinkelstr. 2, 52062 Aachen, Germany
[c] Department of Physical and Theoretical Chemistry, School of Chemistry, University of Nottingham, University Park, Nottingham NG7 2RD, United Kingdom
[d] Sorbonne Universités, Université Paris-Diderot SPC, CNRS, Laboratoire Jacques-Louis Lions, LJLL, F-75005, Paris, France
[e] Institut Universitaire de France, France
[f] Brown University, Division of Applied Mathematics, Providence, RI, USA

ARTICLE INFO

Article history:
Received 1 October 2017
Received in revised form 23 May 2018
Accepted 4 June 2018
Available online 6 June 2018

Keywords:
Electrostatic interaction
Dielectric materials
Many-body
Polarization
Surface charge

ABSTRACT

In this article, a numerical method to compute the electrostatic interaction energy and forces between many dielectric particles is presented. The computational method is based on a Galerkin approximation of an integral equation formulation, which is sufficiently general, as it is able to treat systems embedded in a homogeneous dielectric medium containing an arbitrary number of spherical particles of arbitrary size, charge, dielectric constant and position in the three-dimensional space. The algorithmic complexity is linear scaling with respect to the number of particles for the computation of the energy which has been achieved through the use of a modified fast multipole method. The method scales with the third power of the degree of spherical harmonics used in the underlying expansions, for general three-dimensional particle configurations. Several simple numerical examples illustrate the capabilities of the model, and the influence of mutual polarization between particles in an electrostatic interaction is discussed.

1. Introduction

In computational studies of charged particles, the description of a two-body electrostatic interaction often provides an adequate characterization of underlying physical phenomena. Examples include the investigation of certain aspects of cloud formation [1], the behavior of volcanic ash [2], and the stability of colloidal particles in dilute solutions [3]. Recent years have seen numerous solutions presented to address the problem of calculating electrostatic interactions between pairs of charged particles, covering materials of both dielectric [4–10] and metallic [11] nature. These solutions provide an excellent platform for understanding the fundamental and inherent peculiarities, such as the onset of attractive forces between like-charged particles under certain experimental conditions [12], and they also generate quantitatively accurate results that can be applied to the interpretation of experimental observations [6,13–16].

* Corresponding authors.
E-mail addresses: best@mathcces.rwth-aachen.de (B. Stamm), elena.besley@nottingham.ac.uk (E. Besley).

https://doi.org/10.1016/j.jcp.2018.06.015

However, in many cases a knowledge of two-body forces is not sufficient for a quantitative description of processes that involve interactions between more than two charged particles, and under these circumstances a solution to more complex systems where multiple particles interact would appear necessary. Examples include concentrated colloidal solutions [17], Coulombic crystals [18], electrostatic self-assembly [19] and, more recently, superlattices [20]. Generally, a two-body electrostatic interaction arises when the presence of electric charge in one of the particles creates an electric field that induces a redistribution of surface charge and/or the polarization of bound charge on a second particle, which, in turn, generates its own electric field, thus prompting the same effect on the first particle. This iterative process results in an equilibrium state where both particles acquire a static charged configuration that can be either attractive or repulsive. It is anticipated that if a third particle is introduced to a two-body system, the aforementioned iterative process will take place between all three particles, potentially altering the equilibrium state of the system.

A number of solutions for calculating electrostatic interactions in collections of charged particles are described in the literature, with the majority relying on image charge methods [21–24], and several others on a multipole expansion approach [10,25,26]. The latter method has an advantage of providing a more physical picture of the electrostatic nature of the interaction in terms of how the redistribution of charge takes place. However, an accurate description of electrostatic interactions using these methods often becomes prohibitive in terms of computation time, particularly if the configuration of a model system requires the use of a large number of "images" or multipole terms. Indeed, describing electrostatic interactions in many-body dielectric systems is an intrinsically complex problem, as the induction of bound charges due to polarization effects in one particle is coupled with the same process in all others; as a consequence, each pairwise interaction cannot be resolved independently. In addition, simplification based on symmetry assumptions, that can be naturally imposed on a two-body system, rarely works if three or more particles are involved.

It is common to formulate these problems in terms of an integral equation, often referred to Boundary Integral Equation (BIE), of the second kind following a discretization by means of the Boundary Element Method (BEM) [27–30] which involves a mesh to approximate the geometry and low order basis functions. An alternative strategy is to rely on the basic translation operators of the fast multipole method methodology within the Method of Moments (MoM) [31–36]. Arbitrary shapes can be dealt within the framework of the scattering matrix formalism [37–40], which also allows for construction of highly efficient, general purpose algorithms—in the sense that it's applicable beyond the Laplace case—as in the recent work by Ganesh and Hawkings [41].

In this work, a general solution based on an integral equation approach to the problem of calculating electrostatic interactions between many dielectric spherical particles is presented. The developed solution treats an arbitrary number of particles of arbitrary size, charge, position and dielectric constant, embedded in a homogeneous medium. The method can be classified as a spectral Galerkin approximation of a second kind integral equation and thus stands on a solid mathematical ground through a variational formulation. Since the method is based on a spectral approach on each sphere, exponential convergence is achieved for smooth solutions which is the case in our context. Further, no error is committed in approximating the geometry since no meshing is required, which also allows very efficient discretizations for polydisperse configurations, for example. It therefore combines the variational aspect of the BEM-method with the high order character of the MoM.

The complexity of the presented algorithm scales linearly with respect to the number of particles in the system, which has been achieved through the use of a modified fast multipole method (FMM) due to an equivalence between a surface charge represented by a truncated series of spherical harmonics and a corresponding multipole located at the sphere's center. For a general three-dimensional particle configuration, the complexity scales with the fourth power of the degree of spherical harmonics used in the underlying expansions if no FMM is employed and is reduced to the third power with the more efficient FMM-embedding. This corresponds to the same asymptotic scaling as the method presented in [36]. Further, and in the very particular case when azimuthal symmetry can be assumed, quadratic scaling with the degree of spherical harmonics is obtained.

As presented here, the solution can provide an accurate quantitative description of the physical characteristics of the electrostatic problem, with an important feature of being computationally very efficient. In addition, it converges up to the point where particles touch and can therefore be utilized as a force field for particle dynamics simulations, as presented elsewhere [42].

2. Methodology

2.1. Geometric description and problem formulation

We begin with a geometric description of the system, namely a large collection of charged dielectric spheres. Let $\Omega_1, \ldots, \Omega_M$ be a collection of M non-overlapping spheres in $\mathbb{R}^3$ as illustrated in Fig. 1, where each Ω_i has radius r_i and is centered at $x_i \in \mathbb{R}^3$. The dielectric constant (relative permittivity) within each sphere Ω_i is denoted by $k_i \geq 1$ and, correspondingly, the dielectric constant of the surrounding medium is denoted by $k_0 \geq 1$. The piecewise dielectric constant as a function of space is then given by

$$k(x) = k_0 + \sum_{i \in \{1,\ldots,M\}} (k_i - k_0) \mathbb{1}_{\Omega_i}(x), \qquad x \in \mathbb{R}^3,$$

where $\mathbb{1}_{\Omega_i}$ denotes the characteristic function of Ω_i.

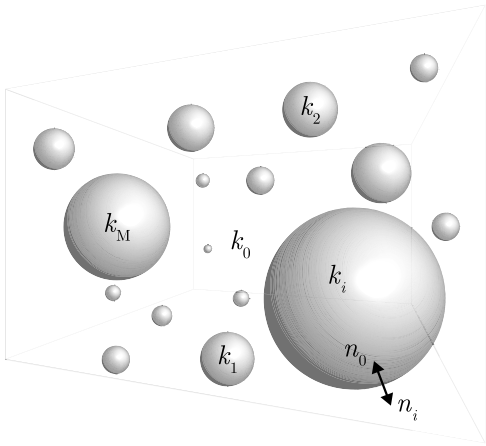

Fig. 1. Geometric representation of a many-body problem.

Let $\Omega_0 = \mathbb{R}^3 \setminus \cup_{i=1}^{M} \overline{\Omega_i}$ be the complementary part to the spheres and set $\Gamma_i = \partial\Omega_i$ for $i = 0, 1, \ldots, M$. Note that

$$\overline{\Omega_0}^c = \Omega_1 \cup \ldots \cup \Omega_M,$$
$$\Gamma_0 = \Gamma_1 \cup \ldots \cup \Gamma_M.$$

We consider the case of electrostatic interaction between dielectric spheres, each carrying a free charge q_i, uniformly distributed over its surface and represented by a surface density $\sigma_{f,i} = q_i/(4\pi r_i^2) \in \mathbb{R}$. Let σ_f denote the global function such that

$$\sigma_f(x) = \begin{cases} \sigma_{f,i} & \text{if } x \in \Gamma_i, \\ 0 & \text{otherwise} \end{cases}.$$

The electrostatic potential $\Phi \in L^2_{\text{loc}}(\mathbb{R}^3)$ with $\Phi|_{\Omega_i} \in H^1(\Omega_i)$ for all $i = 0, 1, \ldots, M$ created by a density of free charge σ_f residing on the spheres satisfies the equation

$$\Delta\Phi = 0 \qquad \text{in each } \Omega_i, i = 0, 1, \ldots, M, \tag{1}$$
$$[\![\Phi]\!] = 0 \qquad \text{on } \Gamma_0, \tag{2}$$
$$[\![k\nabla\Phi]\!] = 4\pi K\sigma_f \qquad \text{on } \Gamma_0, \tag{3}$$

where K denotes Coulomb's constant, and $[\![\Phi]\!]$ and $[\![k\nabla\Phi]\!]$ are jumps defined by

$$[\![\Phi]\!]|_{\Gamma_i}(x) = \Phi|_{\Omega_0}(x)n_0(x) + \Phi|_{\Omega_i}(x)n_i(x),$$
$$[\![k\nabla\Phi]\!]|_{\Gamma_i}(x) = (k\nabla\Phi)|_{\Omega_0}(x) \cdot n_0(x) + (k\nabla\Phi)|_{\Omega_i}(x) \cdot n_i(x),$$

for all $x \in \Gamma_i$, $i = 1, \ldots, M$, and where $n_i(x)$ denotes the outward pointing normal to Ω_i for $x \in \Gamma_i$.

The total electrostatic energy of the system can then be written as

$$U(\Phi, \sigma_f) = \frac{1}{2}\int_{\Gamma_0} \sigma_f(s)\Phi(s)ds. \tag{4}$$

2.2. Representation in terms of integral equations

We now derive an integral equation formulation for the problem described by the partial differential equations (1)–(3). We begin by recalling some basic tools of potential theory (see for example [43]) that are needed in the derivation of the integral equation. In the sequel, $H^s(\Omega)$ and $H^s(\Gamma)$ denote the Sobolev space of order s on the domain Ω or the surface Γ; see [43, Chapter 2] for an introduction.

2.2.1. Local representation

At a local level, i.e., for each sphere Γ_i with $i = 1, \ldots, M$, we first introduce the notion of a local single layer potential $\tilde{\mathcal{S}}_i : H^{-\frac{1}{2}}(\Gamma_i) \to H^1(\mathbb{R}^3 \backslash \Gamma_i)$ which is defined for any sphere Γ_i by

$$(\tilde{\mathcal{S}}_i \sigma_i)(x) := \int_{\Gamma_i} \frac{\sigma_i(s)}{|x-s|}\, ds, \qquad \forall x \in \mathbb{R}^3 \backslash \Gamma_i,$$

for any $\sigma_i \in H^{-\frac{1}{2}}(\Gamma_i)$. Further, any harmonic function w in $\Omega_i \cup \overline{\Omega}_i^c$ that is continuous across the interfaces Γ_i can be represented by the discontinuity in its normal derivative on Γ_i across the interface by the local single layer potential

$$w = \tilde{\mathcal{S}}_i \sigma_i \qquad \text{with} \quad \sigma_i = \frac{1}{4\pi} [\![\nabla w]\!]. \tag{5}$$

Now, the invertible local single layer boundary operator $\mathcal{S}_i : H^{-\frac{1}{2}}(\Gamma_i) \to H^{\frac{1}{2}}(\Gamma_i)$ can be introduced by restricting the single layer potential to Γ_i:

$$(\mathcal{S}_i \sigma_i)(s) = (\tilde{\mathcal{S}}_i \sigma_i)|_{\Gamma_i}(s) = \int_{\Gamma_i} \frac{\sigma_i(s')}{|s-s'|}\, ds', \qquad \forall s \in \Gamma_i.$$

Indeed, the local single layer potential $\tilde{\mathcal{S}}_i$ is continuous across the interface Γ_i and the local single layer boundary operator is invertible.

Assume now that a Dirichlet trace $\lambda_i \in H^{\frac{1}{2}}(\Gamma_i)$ on Γ_i is given, then the harmonic extension in Ω_i can be represented by the single layer potential $\tilde{\mathcal{S}}_i \sigma_i$ in Ω_i where σ_i satisfies the integral equation

$$\mathcal{S}_i \sigma_i = \lambda_i, \qquad \text{on } \Gamma_i. \tag{6}$$

Further, the interior Neumann trace (the outward pointing normal derivative) is given by

$$\nabla w|_{\Omega_i} \cdot n_i = (2\pi + \mathcal{D}_i^\star)\sigma_i, \tag{7}$$

where $\mathcal{D}_i^\star$ is the adjoint operator for the double layer boundary operator which, in turn, is self-adjoint and equal to

$$\mathcal{D}_i^\star = \mathcal{D}_i = -\frac{1}{2r_i}\mathcal{S}_i \tag{8}$$

for the simplified case of a sphere of radius r_i. Therefore, the Dirichlet-to-Neumann map $\mathrm{DtN}_i : H^{\frac{1}{2}}(\Gamma_i) \to H^{-\frac{1}{2}}(\Gamma_i)$, which takes as input the Dirichlet trace λ_i and returns the interior Neumann trace $\nabla w|_{\Omega_i} \cdot n_i$ of the harmonic extension in Ω_i is given by

$$\lambda_i \mapsto \mathrm{DtN}_i(\lambda_i) = \left(2\pi \mathcal{S}_i^{-1} - \frac{1}{2r_i} \right) \lambda_i.$$

2.2.2. Global representation

Since the dielectric constant of the system is piecewise constant, it follows that the problem can be cast as an interface problem. As discussed above on the local level, it follows from potential theory that any function satisfying (1)–(3) can be represented by a global single layer potential

$$\Phi(x) = (\tilde{\mathcal{S}}_{\mathrm{G}} \nu)(x) := \sum_{i \in \{1,\ldots,M\}} (\tilde{\mathcal{S}}_i \nu_i)(x), \tag{9}$$

where $\tilde{\mathcal{S}}_{\mathrm{G}} : H^{-\frac{1}{2}}(\Gamma_0) \to H^1(\mathbb{R}^3 \backslash \Gamma_0)$ is the global single layer potential and

$$\nu_i = \nu|_{\Gamma_i} = \frac{1}{4\pi} [\![\nabla \Phi]\!], \qquad \text{on each } \Gamma_i. \tag{10}$$

This allows the unknown Φ to be represented more economically in terms of ν, which, in turn, yields a more efficient numerical method for this particular example. Indeed, the function ν is only defined on the surface Γ_0. In the following, we will derive an integral equation which determines uniquely the unknown density $\nu \in H^{-\frac{1}{2}}(\Gamma_0)$ by its local pieces ν_i on each Γ_i. We will also refer to the global single layer boundary operator $\mathcal{S}_{\mathrm{G}} : H^{-\frac{1}{2}}(\Gamma_0) \to H^{\frac{1}{2}}(\Gamma_0)$, associated with $\tilde{\mathcal{S}}_{\mathrm{G}}$, and given by $\mathcal{S}_{\mathrm{G}} \nu = (\tilde{\mathcal{S}}_{\mathrm{G}} \nu)|_{\Gamma_0}$.

2.2.3. Integral equation

First, denote the evaluation of Φ at each boundary Γ_i, $i \in \{1, \dots, M\}$, by $\lambda_i \in H^{\frac{1}{2}}(\Gamma_i)$, i.e.

$$\lambda_i(s) = \Phi|_{\Gamma_0}(s) = (\mathcal{S}_{\mathbb{G}}\nu)(s), \qquad \forall s \in \Gamma_i. \tag{11}$$

Second, and as explained above, Φ can be locally represented in Ω_i (and only in Ω_i) by some local density σ_i which is supported only on Γ_i, such that

$$\Phi(x) = (\tilde{\mathcal{S}}_i\sigma_i)(x) := \int_{\Gamma_i} \frac{\sigma_i(s)}{|x-s|} ds, \qquad \forall x \in \Omega_i. \tag{12}$$

The local density σ_i can be determined uniquely by the local integral equation (6) assuming for now that λ_i is known. Having a representation for Φ in the interior of Ω_i, its Neumann trace on Γ_i can be expressed following (7) and (8):

$$\nabla\Phi|_{\Omega_i}\cdot n_i = \left(2\pi - \frac{1}{2r_i}\mathcal{S}_i\right)\sigma_i. \tag{13}$$

Using the discontinuity condition (3), the exterior (to Ω_i) Neumann trace can be shown to be

$$\nabla\Phi|_{\Omega_0}\cdot n_0 = \frac{1}{k_0}(4\pi K\sigma_{f,i} - k_i\nabla\Phi|_{\Omega_i}\cdot n_i) \tag{14}$$

on each Γ_i, $i \in \{1, \dots, M\}$. However, it has already been shown in (9) that the solution Φ can be represented globally by the density ν_i defined in (10) and therefore, it holds locally on each Γ_i that

$$\begin{aligned}\nu_i &= \frac{1}{4\pi}[\![\nabla\Phi]\!]|_{\Gamma_i} = \frac{K}{k_0}\sigma_{f,i} + \frac{k_0-k_i}{4\pi k_0}\nabla\Phi|_{\Omega_i}\cdot n_i = \frac{K}{k_0}\sigma_{f,i} + \frac{k_0-k_i}{4\pi k_0}\left(2\pi - \frac{1}{2r_i}\mathcal{S}_i\right)\sigma_i \\ &= \frac{K}{k_0}\sigma_{f,i} + \frac{k_0-k_i}{4\pi k_0}\left(2\pi - \frac{1}{2r_i}\mathcal{S}_i\right)\mathcal{S}_i^{-1}\lambda_i,\end{aligned}$$

by combining (12)–(14). Recalling (11), we can derive a globally coupled integral equation as given by

$$\left[I_{\mathrm{id}} - \frac{k_0-k_i}{4\pi k_0}\left(2\pi\mathcal{S}_i^{-1} - \frac{1}{2r_i}\right)\mathcal{S}_{\mathbb{G}}\right]\nu = \frac{K\sigma_{f,i}}{k_0} \tag{15}$$

on each Γ_i.

Considering the energy functional, we observe that

$$U(\Phi, \sigma_f) = \frac{1}{2}\int_{\Gamma_0}\sigma_f(s)\lambda(s)\,ds = \frac{1}{2}\sum_{i=1}^{M}\int_{\Gamma_i}\sigma_{f,i}(s)\lambda_i(s)\,ds. \tag{16}$$

Note that the energy is easily computed starting from $\lambda = \mathcal{S}_{\mathbb{G}}\nu$, and not from the ν directly, which is the unknown of equation (15). We can define an equivalent equation for ν by applying $\mathcal{S}_{\mathbb{G}}$ to both sides in (15):

$$\lambda - \mathcal{S}_{\mathbb{G}}\mathcal{L}\lambda = \frac{K}{k_0}\mathcal{S}_{\mathbb{G}}\sigma_f, \tag{17}$$

where the local operator $\mathcal{L}_j$ is defined by

$$(\mathcal{L}\lambda)|_{\Gamma_j} := \mathcal{L}_j\lambda_j, \tag{18}$$

$$\mathcal{L}_j\lambda_j := \frac{k_0-k_j}{4\pi k_0}\left(2\pi\mathcal{S}_j^{-1} - \frac{1}{2r_j}\right)\lambda_j. \tag{19}$$

The integral formulation to the problem consists of solving (17) and then computing the energy following (16).

2.3. Discretization

After a short introduction to the basic elements of real spherical harmonics we will derive a Galerkin discretization of (17) based on series of truncated series of real spherical harmonics.

2.3.1. Real spherical harmonics and quadrature

Denote by $(\mathcal{Y}_{\ell m})_{l\in\mathbb{N},\,-l\le m\le l}$ the set of real spherical harmonics (for the unit sphere $\mathbb{S}^2$ in $\mathbb{R}^3$), normalized in such a way that

$$\langle \mathcal{Y}_{\ell m}, \mathcal{Y}_{\ell' m'}\rangle_{\mathbb{S}^2} = \int_{\mathbb{S}^2} \mathcal{Y}_{\ell m}(s)\,\mathcal{Y}_{\ell' m'}(s)\,ds = \delta_{\ell\ell'}\delta_{mm'}, \tag{20}$$

where $\delta_{n,m}$ denotes the Kronecker delta-function. The spherical harmonics can be extended to the sphere $\partial B_r(x_0)$ with center x_0 and radius r by considering the functions

$$\mathcal{Y}_{\ell m}\left(\frac{x-x_0}{r}\right)$$

and the scaled inner product

$$\langle u, v\rangle_{\partial B_r(x_0)} = \frac{1}{r^2}\int_{\partial B_r(x_0)} u(s)\,v(s)\,ds = \int_{\mathbb{S}^2} u(x_0+rs')\,v(x_0+rs')\,ds'.$$

The set of spherical harmonics on $\partial B_r(x_0)$ is also orthonormal with respect to $\langle\cdot,\cdot\rangle_{\partial B_r(x_0)}$, i.e.

$$\left\langle \mathcal{Y}_{\ell m}\left(\frac{\cdot-x_0}{r}\right), \mathcal{Y}_{\ell' m'}\left(\frac{\cdot-x_0}{r}\right)\right\rangle_{\partial B_r(x_0)} = \langle \mathcal{Y}_{\ell m}, \mathcal{Y}_{\ell' m'}\rangle_{\mathbb{S}^2} = \delta_{ll'}\delta_{mm'}.$$

Note that the purpose of the scaled inner product is to avoid the need to scale the basis functions by the factor $1/r$, so that the same set of basis functions can be used on all spheres with different radii. The system of spherical harmonics is complete in $L^2(\partial B_r(x_0))$ so that any function $u\in L^2(\partial B_r(x_0))$ can be written as

$$u(x) = \sum_{\ell=0}^{+\infty}\sum_{m=-\ell}^{\ell} [u]_\ell^m\,\mathcal{Y}_{\ell m}\left(\frac{x-x_0}{r}\right), \tag{21}$$

with

$$[u]_l^m = \left\langle u, \mathcal{Y}_{\ell m}\left(\frac{\cdot-x_0}{r}\right)\right\rangle_{\partial B_r(x_0)} = \int_{\mathbb{S}^2} u(x_0+rs)\mathcal{Y}_{\ell m}(s)\,ds. \tag{22}$$

Since the integral in (22) can not always be computed exactly, we introduce a quadrature (or numerical integration) scheme by a set $\{s_n,\omega_n\}_{n=1}^{N_g}$ of integration points and weights, respectively, on the unit sphere and define by

$$\langle u, v\rangle_{n,i} := \sum_{n=1}^{N_g}\omega_n u(x_i+r_i s_n)\,v(x_i+r_i s_n). \tag{23}$$

In practice, we use the Lebedev quadrature [44] which can integrate couples of spherical harmonics exactly depending on the number of integration points. We refer to [45,46] for more details.

2.3.2. Galerkin approximation

Let $\mathbb{V}_{N,i}$ be the set of functions spanned by spherical harmonics on Γ_i of maximum degree N:

$$\mathbb{V}_{N,i} = \left\{ \sum_{\ell=0}^{N}\sum_{m=-\ell}^{\ell} [v]_\ell^m\,\mathcal{Y}_{\ell m}\left(\frac{x-x_i}{r_i}\right) \;\middle|\; [v]_\ell^m\in\mathbb{R}\right\}.$$

The (pure and impracticable) Galerkin approximation to (17) is then given by: on each Γ_i, find $\lambda_N|_{\Gamma_i}=\lambda_{N,i}\in\mathbb{V}_{N,i}$ such that

$$\forall v_{N,i}\in\mathbb{V}_{N,i}:\qquad \left\langle \lambda_{N,i}-\mathcal{S}_{\mathbb{G}}\mathcal{L}\lambda_N, v_{N,i}\right\rangle_{\partial B_{r_i}(x_i)} = \left\langle \frac{K}{k_0}\mathcal{S}_{\mathbb{G}}\sigma_f, v_{N,i}\right\rangle_{\partial B_{r_i}(x_i)}.$$

In practice however, the exact scalar product has to be replaced by the quadrature and the problem we are solving reads: on each Γ_i, find $\lambda_N|_{\Gamma_i}=\lambda_{N,i}\in\mathbb{V}_{N,i}$ such that

$$\forall v_{N,i}\in\mathbb{V}_{N,i}:\qquad \left\langle \lambda_{N,i}-\mathcal{S}_{\mathbb{G}}\mathcal{L}\lambda_N, v_{N,i}\right\rangle_{n,i} = \left\langle \frac{K}{k_0}\mathcal{S}_{\mathbb{G}}\sigma_f, v_{N,i}\right\rangle_{n,i}. \tag{24}$$

Since each $\lambda_{N,i}\in\mathbb{V}_{N,i}$, it is represented by a set of coefficients $[\lambda_i]_\ell^m$ so that

$$\lambda_N|_{\Gamma_i}(x) = \lambda_{N,i}(x) = \sum_{\ell=0}^{N} \sum_{m=-\ell}^{\ell} [\lambda_i]_\ell^m \, \mathcal{Y}_{\ell m}\left(\frac{x-x_i}{r_i}\right). \tag{25}$$

Therefore the function λ_N has a discrete representation by means of a vector $\boldsymbol{\lambda} \in \mathbb{R}^{M(N+1)^2}$ consisting of all coefficients $[\lambda_i]_\ell^m$.

The corresponding linear system, denoted here by

$$L\boldsymbol{\lambda} = \boldsymbol{f}, \tag{26}$$

is characterized by the entries of the solution matrix and the right-hand side

$$[L_{ij}]_{\ell\ell'}^{mm'} = \left\langle \delta_{ij}\mathcal{Y}_{\ell'm'} - \mathcal{S}_{\mathbb{G}}\mathcal{L}_j\mathcal{Y}_{\ell'm'}, \mathcal{Y}_{\ell m}\right\rangle_{n,i}, \tag{27}$$

$$[f_i]_\ell^m = \left\langle \frac{K}{k_0}\mathcal{S}_{\mathbb{G}}\sigma_f, \mathcal{Y}_{\ell m}\right\rangle_{n,i}, \tag{28}$$

which are derived as follows.

We now derive the expressions for the solution matrix entries as well as for the right hand side of the linear system. First, observe that the spherical harmonics are eigenfunctions of the local single layer operator $\mathcal{S}_j$, i.e.

$$\mathcal{S}_j\mathcal{Y}_{\ell m} = \frac{4\pi r_j}{2\ell+1}\mathcal{Y}_{\ell m}, \qquad \text{on } \Gamma_j.$$

As a consequence, we obtain

$$(\mathcal{L}_j\mathcal{Y}_{\ell'm'})\left(\frac{x-x_j}{r_j}\right) = \left[\frac{k_0-k_j}{4\pi k_0}\left(2\pi\mathcal{S}_j^{-1} - \frac{1}{2r_j}\right)\mathcal{Y}_{\ell'm'}\right]\left(\frac{x-x_j}{r_j}\right) \tag{29}$$

$$= \ell' \, \frac{k_0-k_j}{4\pi k_0 r_j}\, \mathcal{Y}_{\ell'm'}\left(\frac{x-x_j}{r_j}\right), \tag{30}$$

for all $x \in \Gamma_j$. Second, the single layer potential of $\mathcal{Y}_{\ell'm'}\left(\frac{x-x_j}{r_j}\right)$ in $\mathbb{R}^3\backslash\Omega_i$ is given by

$$(\tilde{\mathcal{S}}_j\mathcal{Y}_{\ell'm'})(x) = \frac{4\pi r_j}{2\ell'+1}\left(\frac{r_j}{|x-x_j|}\right)^{\ell'+1}\mathcal{Y}_{\ell'm'}\left(\frac{x-x_j}{|x-x_j|}\right), \qquad \forall x \in \mathbb{R}^3\backslash\Omega_i. \tag{31}$$

Introducing

$$v_n^{ij} := x_i + r_i s_n - x_j, \qquad s_n^{ij} := \frac{v_n^{ij}}{|v_n^{ij}|} \qquad \text{and} \qquad t_n^{ij} := \frac{|v_n^{ij}|}{r_j},$$

and combining (30) with (31), we obtain

$$(\mathcal{S}_{\mathbb{G}}\mathcal{L}_j\mathcal{Y}_{\ell'm'})(x_i + r_i s_n) = \frac{\ell'}{2\ell'+1}\frac{k_0-k_j}{k_0}(t_n^{ij})^{-(\ell'+1)}\mathcal{Y}_{\ell'm'}(s_n^{ij}). \tag{32}$$

The numerical integration becomes

$$\left\langle \mathcal{S}_{\mathbb{G}}\mathcal{L}_j\mathcal{Y}_{\ell'm'}, \mathcal{Y}_{\ell m}\right\rangle_{n,i} = \sum_{n=1}^{N_g}\omega_n \, \mathcal{Y}_{\ell m}(s_n)\,(\mathcal{S}_{\mathbb{G}}\mathcal{L}_j\mathcal{Y}_{\ell'm'})(x_i + r_i s_n)$$

$$= \frac{\ell'}{2\ell'+1}\frac{k_0-k_j}{k_0}\sum_{n=1}^{N_g}\omega_n \, \mathcal{Y}_{\ell m}(s_n)\,(t_n^{ij})^{-(\ell'+1)}\mathcal{Y}_{\ell'm'}(s_n^{ij}).$$

Therefore, it holds that

$$[L_{ii}]_{\ell\ell'}^{mm'} = \delta_{\ell\ell'}\delta_{mm'}\left(1 - \frac{\ell}{2\ell+1}\frac{k_0-k_i}{k_0}\right) \tag{33}$$

$$[L_{ij}]_{\ell\ell'}^{mm'} = -\sum_{n=1}^{N_g}[L_{ij}^n]_{\ell\ell'}^{mm'}\,(t_n^{ij})^{-(\ell'+1)}\,\mathcal{Y}_{\ell'm'}(s_n^{ij}), \qquad j \neq i, \tag{34}$$

with

$$[L_{ij}^n]_{\ell\ell'}^{mm'} := \omega_n \, \frac{\ell'}{2\ell'+1}\frac{k_0-k_j}{k_0}\,\mathcal{Y}_{\ell m}(s_n).$$

Remark 2.1. In the case $i = j$, we have used an analytic expression, which is possible in this case; but note that numerical integration can be used instead. The two approaches are identical as long as a sufficiently large number of Lebedev integration points is used, such that products of spherical harmonics, each of maximal degree N, are exactly integrated.

For the right-hand side, we similarly obtain

$$[f_i]_\ell^m = [\sigma_{f,i}]_0^0 \frac{4\pi K r_i}{k_0}\delta_{\ell 0} + \frac{K}{k_0}\sum_{\substack{j\in\{1,\dots,M\}\\ j\neq i}}\sum_{n=1}^{N_g}\omega_n(\tilde{\mathcal{S}}_j\sigma_{f,j})(x_i + r_i s_n)\mathcal{Y}_{\ell m}(s_n) \tag{35}$$

$$= [\sigma_{f,i}]_0^0 \frac{4\pi K r_i}{k_0}\delta_{\ell 0} + \sum_{\substack{j\in\{1,\dots,M\}\\ j\neq i}}\frac{4\pi K r_j}{k_0}\sum_{n=1}^{N_g}\omega_n\mathcal{Y}_{\ell m}(s_n)\,[\sigma_{f,j}]_0^0\,(t_n^{ij})^{-1}\,\mathcal{Y}_{00} \tag{36}$$

$$= [\sigma_{f,i}]_0^0 \frac{4\pi K r_i}{k_0}\delta_{\ell 0} + \sum_{\substack{j\in\{1,\dots,M\}\\ j\neq i}}\sum_{n=1}^{N_g}[f_j^n]_\ell^m\,(t_n^{ij})^{-1}, \tag{37}$$

with

$$[f_j^n]_\ell^m := \frac{4\pi K r_j}{k_0}\,\omega_n\,\mathcal{Y}_{\ell m}(s_n)\,[\sigma_{f,j}]_0^0\,\mathcal{Y}_{00}.$$

2.3.3. Energy

Having solved the linear system $L\boldsymbol{\lambda} = \boldsymbol{f}$, the discrete approximation to the energy $U(\Phi, \sigma_f)$ can be computed following (16) as

$$U(\lambda_N, \sigma_f) = \frac{1}{2}\sum_{i=1}^{M}\int_{\Gamma_i}\sigma_{f,i}(s)\lambda_{N,i}(s)ds.$$

We first write $\sigma_{f,i} \in \mathbb{R}$ in terms of spherical harmonics of degree 0, i.e.

$$\sigma_{f,i} = [\sigma_{f,i}]_0^0\,\mathcal{Y}_{00}\left(\frac{x - x_i}{r_i}\right), \qquad \text{with} \qquad [\sigma_{f,i}]_0^0 = 2\sqrt{\pi}\sigma_{f,i}. \tag{38}$$

Then

$$U(\lambda_N, \sigma_f) = \frac{1}{2}\sum_{i=1}^{M}\int_{\Gamma_i}\sigma_{f,i}(s)\lambda_i(s)ds = \langle\boldsymbol{\Psi}, \boldsymbol{\lambda}\rangle, \tag{39}$$

where entries for the vector $\boldsymbol{\Psi}$ are given by

$$[\Psi_i]_\ell^m = \delta_{\ell 0}\frac{r_i^2}{2}[\sigma_{f,i}]_0^0$$

and

$$\langle\boldsymbol{\Psi}, \boldsymbol{\lambda}\rangle := \sum_{i\in\{1,\dots,M\}}\sum_{\ell=0}^{N}\sum_{m=-\ell}^{\ell}[\Psi_i]_\ell^m[\lambda_i]_\ell^m.$$

This corresponds to the total energy of the system. In order to study the interaction energy of the system, we first define for each Γ_i the solution to (1)–(3) but only for a single sphere Γ_i, neglecting the presence of all other spheres in the geometrical configuration. Thus, the solution on Γ_i, denoted here by $\lambda_{f,i}$, is given by

$$\lambda_{f,i} = \frac{K}{k_0}\mathcal{S}_i\sigma_{f,i},$$

such that the total self-energy of the system, given by the sum of the individual self-energies (Born energies), is defined as

$$U^{\text{self}}(\sigma_f) = \frac{1}{2}\sum_{i=1}^{M}\int_{\Gamma_i}\sigma_{f,i}(s)\lambda_{f,i}(s)ds = \langle\boldsymbol{\Psi}, \boldsymbol{\lambda}_f\rangle. \tag{40}$$

Here, entries for the vector $\boldsymbol{\lambda}_f$ are given by

$$[\lambda_{f,i}]_\ell^m = \delta_{\ell 0}\frac{4\pi r_i K}{k_0}[\sigma_{f,i}]_0^0.$$

The interaction energy is then given as the difference between the total energy and the self-energy of the system:

$$U^{\text{int}}(\lambda_N, \sigma_f) = U(\lambda_N, \sigma_f) - U^{\text{self}}(\sigma_f).$$

2.3.4. Force

The force acting on each of the spheres Γ_k is the gradient of the (discrete) energy with respect to changes in the location of the center $x_k = (x_k^1, x_k^2, x_k^3)$ of Γ_k, that is

$$F_k^\alpha = -\partial_{x_k^\alpha} U(\lambda_N, \sigma_f) = -\partial_{x_k^\alpha}\langle \boldsymbol{\Psi}, \boldsymbol{\lambda}\rangle = -\langle \boldsymbol{\Psi}, \partial_{x_k^\alpha}\boldsymbol{\lambda}\rangle,$$

where $\partial_{x_k^\alpha} = \frac{\partial}{\partial x_k^\alpha}$ for $\alpha = 1, 2, 3$. Note first that all $\sigma_{f,i}$ and thus Ψ do not depend on any position x_k of the sphere Γ_k, and second, the self-energy $U^{\text{self}}(\sigma_f)$ is also independent of x_k.

Considering now the linear system $L\boldsymbol{\lambda} = \boldsymbol{f}$, the derivative with respect to x_k on both sides yields

$$\partial_{x_k^\alpha}(L\boldsymbol{\lambda}) = (\partial_{x_k^\alpha} L)\boldsymbol{\lambda} + L(\partial_{x_k^\alpha}\boldsymbol{\lambda}) = \partial_{x_k^\alpha}\boldsymbol{f}.$$

Regrouping the terms yields

$$L(\partial_{x_k^\alpha}\boldsymbol{\lambda}) = \partial_{x_k^\alpha}\boldsymbol{f} - (\partial_{x_k^\alpha} L)\boldsymbol{\lambda} =: \boldsymbol{h}_k^\alpha. \tag{41}$$

Then,

$$F_k^\alpha = -\langle \boldsymbol{\Psi}, L^{-1}\boldsymbol{h}_k^\alpha\rangle = -\langle L^{-T}\boldsymbol{\Psi}, \boldsymbol{h}_k^\alpha\rangle = -\langle \boldsymbol{s}, \boldsymbol{h}_k^\alpha\rangle,$$

where $\boldsymbol{s}$ is a solution to the adjoint system

$$L^T\boldsymbol{s} = \boldsymbol{\Psi}. \tag{42}$$

Thus the force acting on the k-th sphere is given by

$$F_k = (F_k^1, F_k^2, F_k^3).$$

This approach is very efficient as the dual problem needs to be solved only once and not for each k.

It remains to characterize the different coefficients of $\boldsymbol{h}_k^\alpha$. Applying the chain rule implies for all $k = \{1, \dots, M\}$:

$$\begin{aligned}
\partial_{x_k^\alpha}[L_{ii}]_{\ell\ell'}^{mm'} &= 0\\
\partial_{x_k^\alpha}[L_{ij}]_{\ell\ell'}^{mm'} &= -\sum_{n=1}^{N_g}[L_{ij}^n]_{\ell\ell'}^{mm'}\,\partial_{x_k^\alpha}\left((t_n^{ij})^{-(\ell'+1)}\,\mathcal{Y}_{\ell' m'}(s_n^{ij})\right)\\
&= -\sum_{n=1}^{N_g}[L_{ij}^n]_{\ell\ell'}^{mm'}\,(t_n^{ij})^{-(\ell'+1)}\left(\partial_{x_k^\alpha}\mathcal{Y}_{\ell' m'}(s_n^{ij}) - (\ell'+1)(t_n^{ij})^{-1}\,(\partial_{x_k^\alpha} t_n^{ij})\,\mathcal{Y}_{\ell' m'}(s_n^{ij})\right), \qquad j \neq i,
\end{aligned}$$

and

$$\partial_{x_k^\alpha}[f_i]_\ell^m = -\sum_{\substack{j\in\{1,\dots,M\}\\ j\neq i}}\sum_{n=1}^{N_g}[f_j^n]_\ell^m\,(t_n^{ij})^{-2}(\partial_{x_k^\alpha} t_n^{ij}).$$

Note that

$$\partial_{x_k^\alpha} t_n^{ij} = \frac{1}{r_j}\partial_{x_k^\alpha}|v_n^{ij}|,$$

and thus, using the notation $v_n^{ij} = ((v_n^{ij})_1, (v_n^{ij})_2, (v_n^{ij})_3)$, we obtain

$$\partial_{x_k^\alpha}|v_n^{ij}| = \partial_{x_k^\alpha}\left(\sum_{\beta=1}^{3}(v_n^{ij})_\beta^2\right)^{\frac{1}{2}} = \frac{(v_n^{ij})_\alpha}{|v_n^{ij}|}\partial_{x_k^\alpha}(x_i + r_i s_n - x_j)_\alpha = \frac{(v_n^{ij})_\alpha}{|v_n^{ij}|}f_{ijk},$$

where

$$f_{ijk} = \begin{cases} 1 & \text{if } k = i \neq j \\ -1 & \text{if } k = j \neq i \\ 0 & \text{if } k = i = j \\ 0 & \text{if } k \neq i \text{ and } k \neq j \end{cases}.$$

Further computations show that

$$\partial_{x_k^\alpha} \mathcal{Y}_{\ell' m'}(s_n^{ij}) = \frac{1}{|v_n^{ij}|} \partial_{s^\alpha} \mathcal{Y}_{\ell' m'}(s_n^{ij}) \partial_{x_k^\alpha} v_n^{ij} = \frac{1}{|v_n^{ij}|} \partial_{s^\alpha} \mathcal{Y}_{\ell' m'}(s_n^{ij}) f_{ijk},$$

where $\partial_{s^\alpha} \mathcal{Y}_{\ell' m'}(s_n^{ij})$ denotes the α-component of the gradient in Cartesian coordinates of $\mathcal{Y}_{\ell' m'}(s)$ for $s \in \mathbb{S}^2$.

2.4. Fast multipole method implementation

The computation of one matrix–vector product $L\boldsymbol{\lambda}$ scales as $\mathcal{O}(M^2)$ due to the global potential $\mathcal{S}_\mathbb{G}$ in (24), which, in turn, shows that the matrix L is dense. We explain here how an adaptation of a Fast Multipole Method (FMM) [47,48] can be employed to reduce the computational cost of a matrix–vector product involving L and L^T and effectively scales linearly with respect to M. Recall that the adjoint linear system (42) needs to be solved in order to compute the forces acting on the spheres. [39] In order to treat L and L^T simultaneously, we first rewrite L as

$$L = I - \Lambda S \Sigma$$

where Λ, Σ are diagonal, and thus local, matrices with entries

$$[\Lambda_{ii}]_{\ell\ell}^{mm} = \frac{1}{r_i^2} \quad \text{and} \quad [\Sigma_{ii}]_{\ell\ell}^{mm} = \ell \frac{k_0 - k_i}{k_0} \frac{r_i}{4\pi}.$$

The resulting dense matrix S is given by

$$[S_{ij}]_{\ell\ell'}^{mm'} = \frac{r_i^2}{r_j^2} \left\langle \mathcal{S}_\mathbb{G} \mathcal{Y}_{\ell' m'}|_{\Gamma_j}, \mathcal{Y}_{\ell m} \right\rangle_{n,i} = \frac{r_i^2}{r_j^2} \left\langle \tilde{\mathcal{S}}_j \mathcal{Y}_{\ell' m'}, \mathcal{Y}_{\ell m} \right\rangle_{n,i}.$$

The motivation is that, on the continuous level, the single layer operator $\mathcal{S}_\mathbb{G}$ is self-adjoint on Γ_0 using the usual $L^2(\Gamma_0)$ scalar product (and not the scaled version). In consequence, it can be verified that the dense matrix S is approximately symmetric in the sense that it is symmetric when the numerical integration becomes exact. Therefore, the transpose of L can be approximated by

$$L^T \approx I - \Sigma S \Lambda,$$

where the error only depends on the error in numerical integration.

Similar as done for (27) in combination with (23), we derive

$$\begin{aligned} [(S\boldsymbol{\lambda})_i]_\ell^m &= \sum_{j \in \{1,\dots,M\}} \sum_{\ell'=0}^{N} \sum_{m'=-\ell'}^{\ell'} [S_{ij}]_{\ell\ell'}^{mm'} [\lambda_j]_{\ell'}^{m'} = \sum_{j \in \{1,\dots,M\}} \sum_{\ell'=0}^{N} \sum_{m'=-\ell'}^{\ell'} \frac{r_i^2}{r_j^2} \left\langle \tilde{\mathcal{S}}_j \mathcal{Y}_{\ell' m'}, \mathcal{Y}_{\ell m} \right\rangle_{n,i} [\lambda_j]_{\ell'}^{m'} \\ &= \sum_{n=1}^{N_g} \omega_n \mathcal{Y}_{\ell m}(s_n) \sum_{j \in \{1,\dots,M\}} \sum_{\ell'=0}^{N} \sum_{m'=-\ell'}^{\ell'} \frac{r_i^2}{r_j^2} (\tilde{\mathcal{S}}_j \mathcal{Y}_{\ell' m'})(x_i + r_i s_n) [\lambda_j]_{\ell'}^{m'} \\ &= r_i^2 \sum_{n=1}^{N_g} \omega_n \mathcal{Y}_{\ell m}(s_n) \, \Phi(x_i + r_i s_n), \end{aligned}$$

with

$$\Phi(x) = \sum_{j \in \{1,\dots,M\}} \frac{1}{r_j^2} \sum_{\ell'=0}^{N} \sum_{m'=-\ell'}^{\ell'} [\lambda_j]_{\ell'}^{m'} (\tilde{\mathcal{S}}_j \mathcal{Y}_{\ell' m'})(x).$$

Applying (31), we further develop

$$\Phi(x) = \sum_{j\in\{1,\dots,M\}} \frac{1}{r_j^2} \sum_{\ell'=0}^{N} \sum_{m'=-\ell'}^{\ell'} [\lambda_j]_{\ell'}^{m'} \frac{4\pi r_j}{2\ell'+1} \left(\frac{r_j}{|x-x_j|}\right)^{\ell'+1} \mathcal{Y}_{\ell' m'}\left(\frac{x-x_j}{|x-x_j|}\right) \tag{43}$$

$$= \sum_{j\in\{1,\dots,M\}} \sum_{\ell'=0}^{N} \sum_{m'=-\ell'}^{\ell'} [\Phi_j]_{\ell'}^{m'} \frac{1}{|x-x_j|^{(\ell'+1)}} \mathcal{Y}_{\ell' m'}\left(\frac{x-x_j}{|x-x_j|}\right) \tag{44}$$

with

$$[\Phi_j]_{\ell'}^{m'} = \frac{4\pi}{2\ell'+1} r_j^{\ell'} [\lambda_j]_{\ell'}^{m'}.$$

Therefore, evaluating Φ at all integration points $x_i + r_i s_n$ on each sphere $i \in \{1,\dots,M\}$ can be interpreted as evaluating the potential of M multipoles which are located at x_j with multipolar moments $[\Phi_j]_{\ell'}^{m'}$ at the integration points $x_i + r_i s_n$.

We note that, as explained in Remark 2.1, the expression (34) for $i = j$ approximates the value of (33) by numerical integration, and it is exact for a large enough number of Lebedev points. We therefore only use expression (34) even for $i = j$ if we use the FMM-framework.

Standard FMM-libraries do not consider arbitrary multipolar expansions as input. Typically, only point-charges are considered, although in some cases dipoles can also be treated. Since the degree N of spherical harmonics is arbitrary in the work presented here, such standard libraries can not be used. However, libraries can be adapted with some effort. Accordingly, we have modified the library ScalFMM [49] as explained in the following. Let P denote the degree of spherical harmonics used in the FMM, then, relying on standard notation within the FMM-framework, see [50] for example, the following changes need to be introduced:

- Replace the P2M-operator by a M2M-operator, which maps each multipolar expansion of the form (44) (thus of degree N) at the scattered locations $\{x_j\}_{j=1}^{M}$ in each box to a multipolar expansion of degree P centered at the box. The P2M-operator is in this case a special case of $N = 0$.
- Replace the P2P-operator by a M2P-operator according to the evaluation of (44).

Once these changes are introduced, one can use the FMM-framework to obtain a linear scaling algorithm for each matrix–vector product $L\boldsymbol{\lambda}$ within an iterative solution algorithm, such as GMRes for example, to solve the linear system (26) as well as the adjoint linear system (42) providing linear scaling for the computation of the interaction energy. We will analyze the performance of the algorithm, and in particular the FMM, in the next section.

3. Numerical results

In the following a series of benchmark tests are first presented, covering the performance of the code as a function of the number of particles (M) and the degree of spherical harmonics (N) utilized in the truncated series. Afterwards, the focus is turned to the presentation of a number of basic examples of many-body interaction that clearly illustrate the capability of the model introduced in this paper. In the first series of examples, the number of particles has been restricted to $M = 3$ to retain clarity of interpretation. For simplicity, various physical quantities involved in these calculations are taken to be dimensionless, with the Coulomb's constant being replaced by unity. Finally, an example with a large number of spheres is presented, in the form of a calculation for the halite ('rock salt') lattice of sodium chloride (NaCl) and an estimation of its Madelung constant. In all calculations of the electrostatic force, the convention of a negative value denoting an attractive force and a positive value denoting an repulsive force is adopted.

3.1. Timing and scaling

The model introduced in section 2 has been implemented in a MATLAB code, and the performance of the later is discussed next, particularly with respect to scaling properties as a function of the number of spheres M and the degree of spherical harmonics N utilized in the truncated series. The FMM-framework is based on the ScalFMM-library which is called from MATLAB by means of the MATLAB MEX-compiler. In this way, the computationally most expensive part is externalized and complied C++ code is actually called from MATLAB. All timing calculations have been performed on a single desktop-class computer, with a Intel Core i7-3820@3.60 GHz processor, 16 GB of DDR3@1333 MHz, running a GNU/Linux based operating system. Since computation time can be sensitive to background activities of the operating system, the calculations were repeated ten times, hence standard deviations are shown as error bars in the resulting figures.

To address the behavior of the code with respect to the number of spheres, a system that grows linearly with the progressive addition of identical spheres is considered first, and the results are plotted in Fig. 2. A calculation for systems with a large number of spheres benefits from the implementation of the Fast Multipole Method (FMM), introduced in section 2.4. When the number of spheres is small, a calculation that does not implement the FMM performs better; however, as the number of spheres in the system increases, a crossover between the two curves occurs at about $M = 50$ (for this

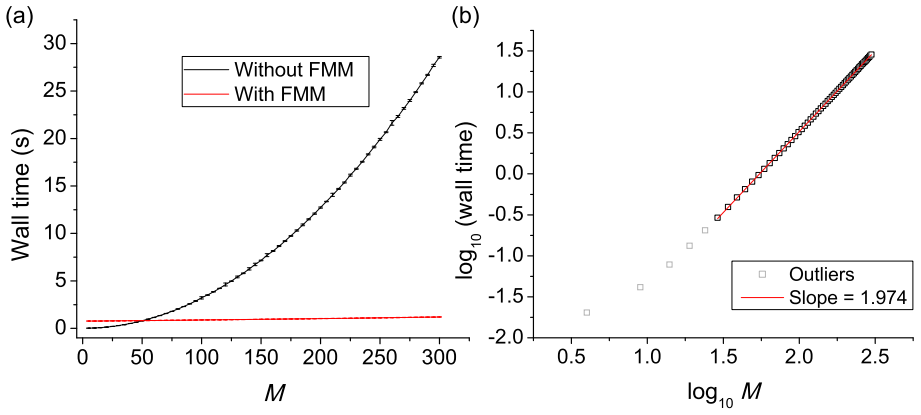

Fig. 2. (a) The wall time (elapsed real time) as a function of the number of spheres M in the system. Although virtually indistinguishable, the elapsed time in the FMM calculation varies from ≈ 0.8 to 1.2 seconds as M increases; (b) log–log plot of the calculation performed without FMM, showing a quadratic scaling profile.

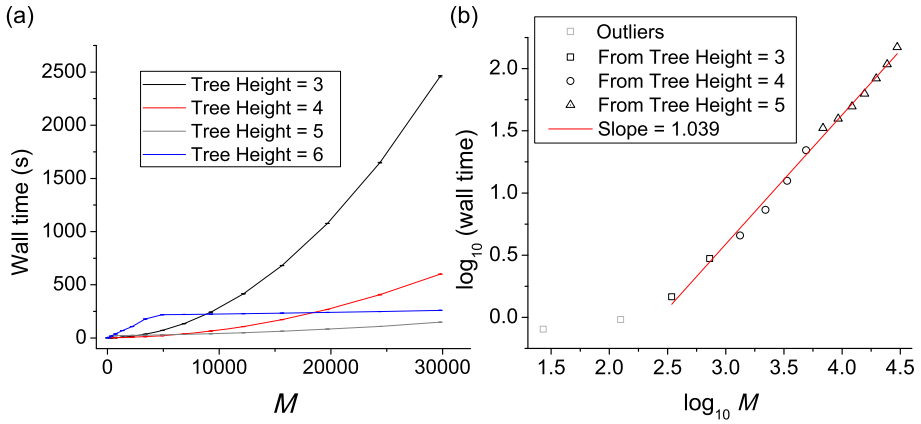

Fig. 3. (a) The wall time as a function of the number of spheres M in the system, for various curves representing different Tree Heights in the FMM calculation; (b) log–log plot of the piecewise composition of parabolic profiles, each corresponding to a particular value of Tree Height, showing that a regular effective linear scaling can be obtained. (For interpretation of the colors in the figure(s), the reader is referred to the web version of this article.)

particular example), and the FMM calculation becomes faster. Fig. 2(b) clearly shows that the calculation scales quadratically when FMM is not used.

A subtle detail of the FMM-algorithm is that it is based on an octree-structure of the bounding box containing all particles where the finest granularity determines the separation between the far-field and the near-field. As the number of dielectric spheres in the system grows, one needs to carefully adapt the number of levels in the octree so that the number of spheres remains asymptotically uniform in the leaves in order to prevent the near-field computations growing quadratically. In consequence, linear scaling can only be achieved if the number of levels is adapted to the number of spheres in the leaves. Accordingly, a quasi-linear curve that is in reality a piecewise composite of quadratic profiles, each corresponding to a different Tree Height, can be obtained. To illustrate this, consider a system that assumes the halite cubic structure of sodium chloride, where each positive particle is surrounded by six negative particles and vice versa. For simplicity, the spheres were made identical with regard to their dielectric constant, size and charge. As shown in Fig. 3(a), each level of Tree Height performs best at a particular segment of the x-axis, being surpassed by the next level when the magnitude of M has increased sufficiently. Fig. 3(b) shows the quasi-linear curve obtained by combining each segment calculated with the optimum corresponding Tree Height.

The behavior of the code with respect to the degree of spherical harmonics N utilized in the truncated series is accessed in Fig. 4, where a three particle case shown later in Fig. 7 is considered. Since this particular case exhibits a perfect linear geometry, an additional simplification can be imposed from the azimuthal symmetry of the system, which is that the spherical harmonics utilized in the truncated series present no ϕ-dependence so that only the terms with $m = 0$ matter for all ℓ. For the majority of problems, however, this later simplification cannot be made and the full set of spherical harmonics needs to be considered. Fig. 4(a) illustrates the Wall time of the calculations with and without exploiting the azimuthal symmetry. While the calculation where the full set of spherical harmonics is considered scales as N^4, the use of symmetry reduces it to a quadratic scaling, as shown in Fig. 4(b). In absolute terms, the use of high orders of spherical harmonics inevitably causes

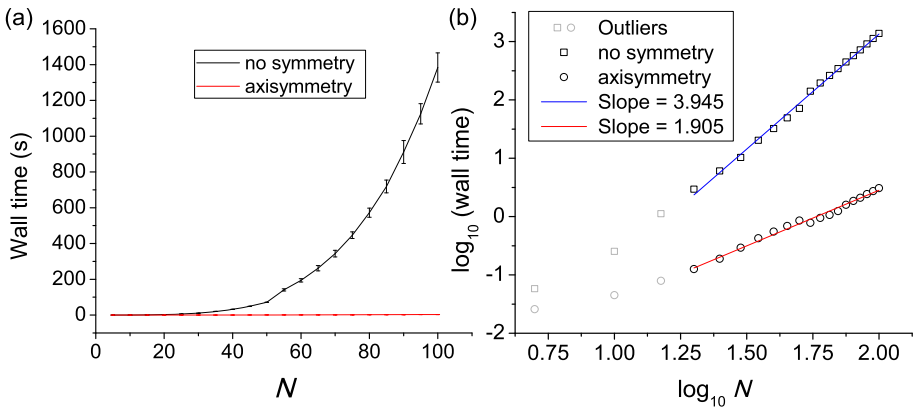

Fig. 4. (a) The wall time as a function of the degree of spherical harmonics utilized in the truncated series. Although virtually indistinguishable, the elapsed time in the axisymmetric calculation varies from ≈ 0.03 to 3 seconds; (b) log–log plot of both curves showing that an imposition of symmetry reduces the scaling profile from $\approx N^4$ to N^2.

the code to run considerably slower, especially when no symmetry can be imposed. The quartic scaling in N corresponds to a quadratic scaling in the number of degrees of freedom per sphere which is a natural scaling for a spherical harmonics Spectral method discretizing a two-dimensional manifold. However, the situations, where the use of such high orders is required, are, in fact, limited. For two-body systems, it has been shown already [51], considering a particular convergence criterion, how the required number of terms in a truncated series generally depends on parameters of the system, namely the particles' dielectric constant, charge and radius, and the inter-particle separation distance. The conclusions from this study can be extrapolated to a many-body system, if one takes into account each pairwise interaction separately. Generally, higher-order terms are required if the separation between any two particles is very small (approximately one tenth of the radii or less), if the ratio of radii and the ratio of dielectric constants are sufficiently large, or if a combination of both these conditions is present.

These were considerations for configurations with only a few particles. If one considers larger systems where the FMM is employed, the scaling with respect to N is determined by the degree of spherical harmonics that is used within the FMM to represent the local and multipolar expansions. We use the FMM with an internal degree of spherical harmonics that is proportional to N, which then results in a cubic scaling of the algorithm with respect to N.

3.2. Nonadditivity of the electrostatic force in many-body systems

As Coulomb's law obeys the principle of superposition, for the case of a system containing any number of uniformly charged non-polarizable spherical particles, it is straightforward to recognize that the total electrostatic force acting on a specific particle is equal to the sum of forces corresponding to pairwise interactions between such particle and all other particles in the system.

Consider the case of three particle interaction depicted in Fig. 5, where each particle is positioned at a vertex of an equilateral triangle. All particles are non-polarizable ($k_1 = k_2 = k_3 = 1$), equal-sized with a nominal radius of 1, and separated by a distance $s = 1$; the yellow particle has a nominal charge of 10, and the dark blue particles have a nominal charge of -10. The top panel in Fig. 5 presents isolated pair interactions, below which the overall interaction between three particles is shown. In this case, the x and y components of the total force acting on each particle are the sum of the x and y components of the force due to the corresponding pair interactions. Therefore, for a system consisting of non-polarizable particles or point charges, the principle of superposition holds and the force is said to be additive.

Consider now the case illustrated in Fig. 6, which has the same parameters as the system addressed in Fig. 5, except for the dielectric constant of the particles, which is now equal to 20. Contrary to the previous case, where the particles are non-polarizable, Fig. 6 shows that when the particles have the ability to be polarized, the electrostatic force does not obey the principle of superposition and becomes nonadditive. Accordingly, in each of the isolated pair interactions, depicted in the upper panel in Fig. 6, two particles become polarized by one another and assume a surface charge distribution that corresponds to the equilibrium configuration. However, when a third particle is added to the system it disrupts the distribution of charge on the pair, and the system as a whole assumes a new equilibrium distribution of surface charge, as shown in the lower panel in Fig. 6. In other words, the charge distribution on a particle in a pair interaction differs from that in the presence of additional particles, which leads to modification of the force components so that the electrostatic force is now characterized as nonadditive. This is evident from Fig. 6 in which the actual force is compared to the force predicted for the case when the principle of superposition is obeyed. Such behavior of the electrostatic force is similar to the induction component of intermolecular forces, which is recognized as being strongly nonadditive [52].

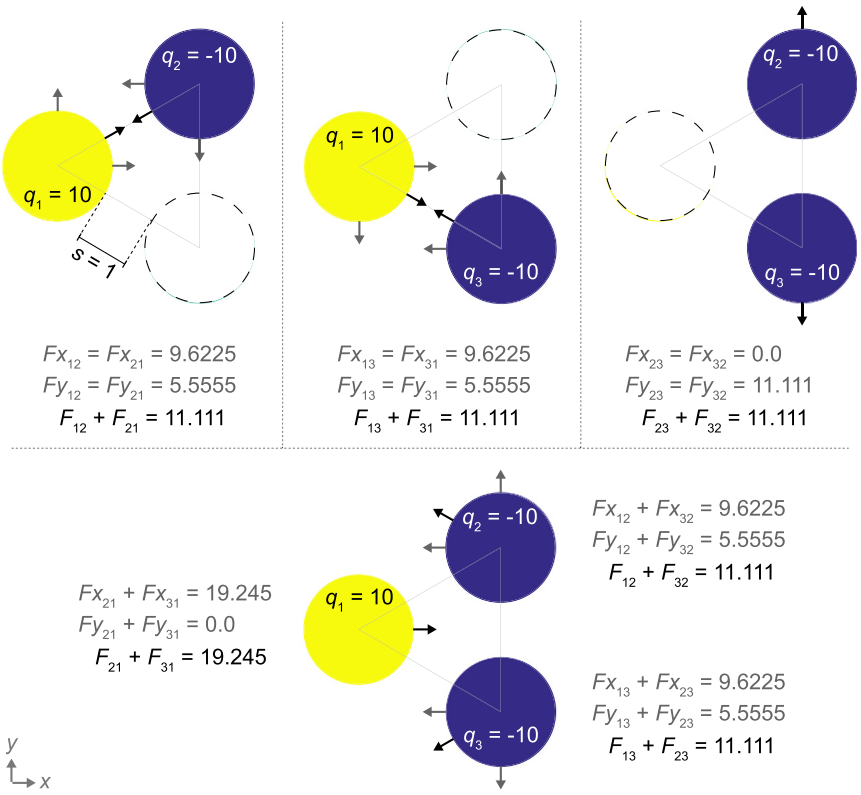

Fig. 5. Schematic illustration of the electrostatic interaction between three non-polarizable particles placed at the vertices of an equilateral triangle of side $h = 3$. The three upper diagrams represent isolated pairwise interactions in the absence of the third particle, whose phantom location is shown as a dashed circle, and the bottom diagram represents the overall interaction, involving all three particles. The values of the x and y components of the force are shaded in grey, while the total force is denoted in black. Accordingly, the arrows represent unit vectors depicting the direction of the force (black) and each component (grey).

3.3. Neutral–charged particle interaction

In a neutral particle − charged particle interaction, the existence of electrostatic effects depends on polarizability of the neutral particle, which must have the dielectric constant k greater than unity. Consider the case shown in Fig. 7, where three particles are placed in a linear geometry, the central particle carries a positive charge and two neutral particles are equidistant on either side. When the particles have the dielectric constant of $k = 1$, i.e. when they are non-polarizable, no bound charge is induced. As the value of k is gradually increased, i.e. as the particles become more polarizable, bound charge is induced and the interactions become progressively more attractive. The surface charge density map in Fig. 7 shows that the electric field created by the positive free charge on the central particle induces negative bound charge on the left- and right-hand particles, particularly in the areas of close proximity to the central particle. Since the left and right particles are neutral their total charge remains zero and the off-set of positive bound charge emerges on the hemisphere facing away from the central particle. The electric fields created by the induced bound charges on the left and right particles also polarize the central particle, which becomes more positively charged in the areas of close proximity to the neighboring neutral particles. The overall effect is that the total force on the left particle is attractive and directed towards the other two particles. By symmetry, the total force on the right particle is also attractive and acting with equal magnitude in the opposite direction; the total force on central particle is zero.

3.4. Opposite-charge interaction

In this second example, shown in Fig. 8, three interacting particles in a linear configuration are charged. The central particle is positively charged, and the two particles on either side are equidistant and carry negatives charge. If the particles are non-polarizable ($k = 1$), the electrostatic interaction is always attractive and described accurately by Coulomb's law. If k is greater than unity bound charges are induced on the particles, similar to the case shown in Fig. 7, and as the value of k is increased the interaction becomes more attractive. For the case shown in Fig. 8(b) the central particle carries significantly less charge than the other two particles showing that a critical value of k is now required for the onset of an attractive interaction. If $k \leq 10$, the combination of an opposite (free) charge interaction and additional attraction due to polarization effects is not sufficient to balance the repulsion between the negative free charges on the left- and right-hand particles;

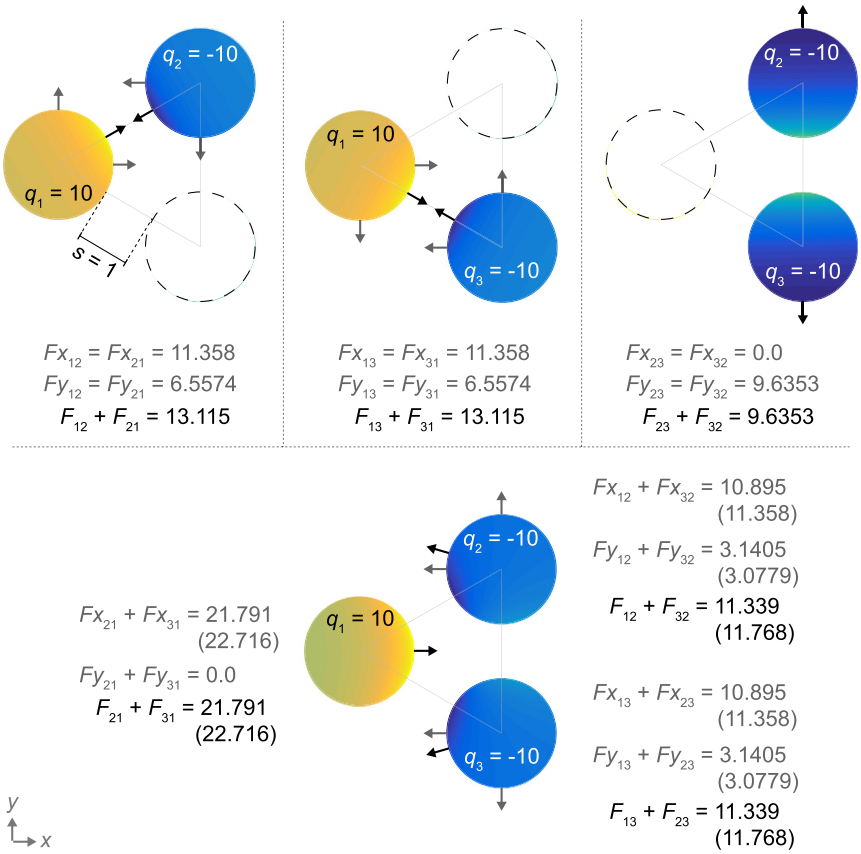

Fig. 6. Schematic illustration of the electrostatic interaction between three polarizable particles with dielectric constants $k_1 = k_2 = k_3 = 20$. Distribution of the total surface charge density is shown by variation of color. The values of the x and y components of the force are shaded in grey, while the total force is denoted in black. The values in brackets give the absolute magnitude of the force if the principle of superposition was obeyed.

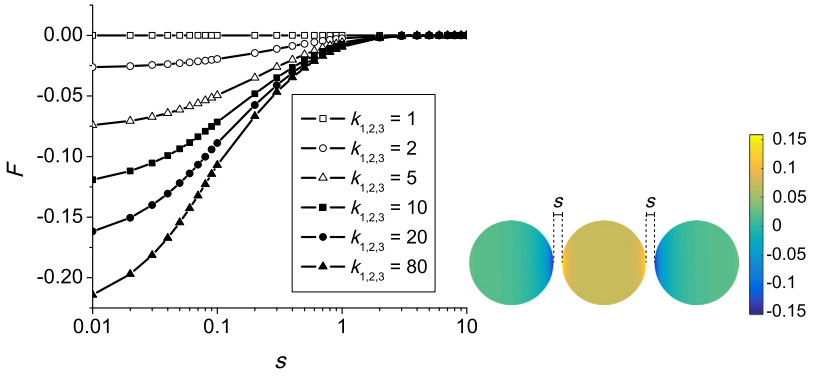

Fig. 7. The total electrostatic force F acting on the left particle as a function of the surface-to-surface separation s and the dielectric constant of the particles, for the case of neutral (green) – charged (yellow) particle interaction. The particle at the center has a nominal charge of $+1$, whilst the left- and right-hand particles are neutral; the particles are equal-sized, with a nominal radius of 1. Also shown is a linear geometry of three body interaction, with the total surface charge density (charge per unit area) mapped out on each particle for the case of $k_1 = k_2 = k_3 = 20$ and $s = 0.2$.

therefore, the overall force on the left-hand particle is repulsive. However, when $k \geq 20$, polarization effects dominate and promote the onset of an overall attractive interaction at sufficiently short inter-particle separation. As in the previous example, in all cases due to symmetry the total force on the central particle remains zero, but the force on the left- and right-hand particles, which has the same magnitude and acts in opposite directions, changes.

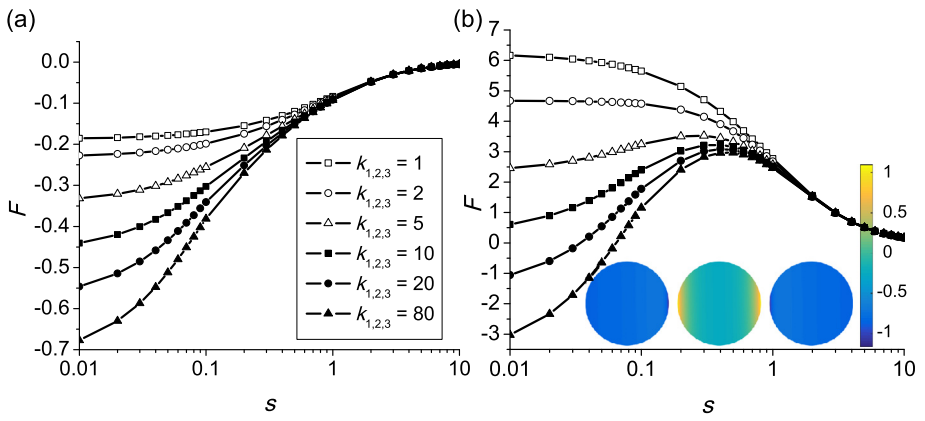

Fig. 8. The total electrostatic force F acting on the left particle as a function of the surface-to-surface separation s and the dielectric constant of the particles, for a case of opposite-charge interaction: (a) the central particle has a nominal charge of $+1$, and the left- and right-hand particles have a nominal charge of -1; (b) the central particle has a nominal charge of $+0.01$, and the left and right particles have a nominal charge of -10. The particles are equal-sized, with a nominal radius of 1. Inset in (b) shows a linear geometry of three body interaction, with the total surface charge density mapped out on each particle for the case of $k_1 = k_2 = k_3 = 20$ and $s = 0.2$.

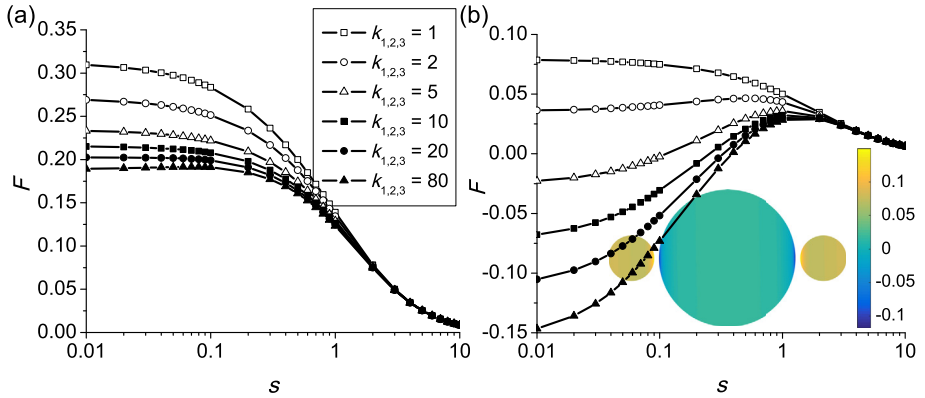

Fig. 9. The total electrostatic force F acting on the left particle as a function of the surface-to-surface separation s and the dielectric constant of the particles, for the case of like-charge interaction between three particles in linear geometry: (a) particles are identical, with a nominal charge of $+1$ and nominal radius of 1; (b) particles have a nominal charge of $+1$, the central particle has a radius of 3, and the left and right particles have a radius of 1. Inset in (b) shows a linear geometry of three body interaction, with the total surface charge density mapped out on each particle for the case of $k_1 = k_2 = k_3 = 20$ and $s = 0.2$.

3.5. Like-charge interaction

Finally, consider the case of three interacting particles placed in a linear configuration, where they all carry a net positive charge, i.e. they are like-charged. Fig. 9(a) shows that when the particles are identical, which includes the magnitude and sign of charge, the electrostatic interaction is always repulsive no matter how polarizable the particles are. In this case, polarization effects merely serve to weaken the electrostatic repulsion between particles. Therefore, as k increases the magnitude of the repulsive force decreases, and by changing one of the parameters of the problem this behavior can be moderated. For example, in Fig. 9(b) the central particle is three times larger than the particles on each side, so the particles have different distribution of surface charge. Higher charge density on the smaller particles induces negative bound charge on the central particle, especially in the areas closest to either particle. In contrast, the particles on each side become more positively charged in the areas nearest to the central particle. The overall effect is that, at sufficiently short separations, an overall attractive interaction between the particles prevails, even though they are all like-charged. A similar scenario involving only two particles has been described elsewhere [5,51].

Fig. 10 also addresses an example of like-charge interaction, but this time the particles are placed in a triangular geometry. Similar to the linear case, the particles are identical, with the result that the electrostatic interaction is always repulsive, with polarization merely weakening the magnitude of the repulsion. However, variation in one of the parameters, in this case the amount of charge on each particle, leads to the emergence of an attractive interaction at sufficiently short separations, as shown in Fig. 10(b). Note that polarization effects are only significant at short separation distances; typically, the dipole, quadrupole, octupole and higher order multipole interactions diminish more rapidly than the monopole (Coulomb) term as the separation between particles increases. Whilst the monopole contribution to the force is inversely proportional

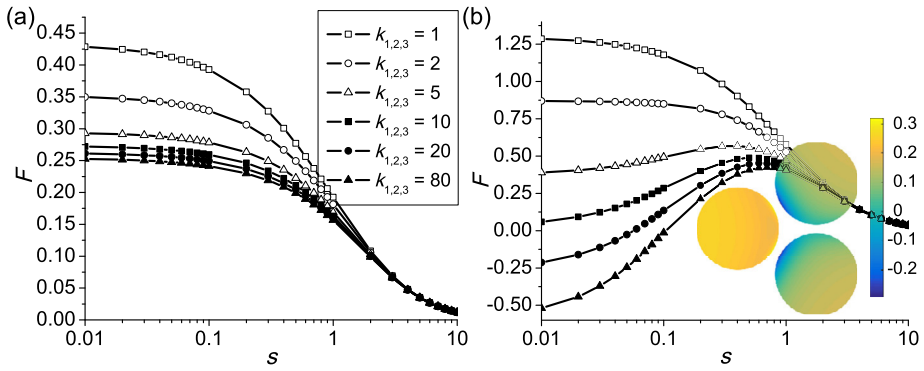

Fig. 10. The total electrostatic force F acting on the left particle as a function of the surface-to-surface separation s, for the case of like-charge interaction between three particles in triangular geometry: (a) particles are identical, with a nominal charge of $+1$ and nominal radius of 1; (b) particles have a nominal radius of 1, the left particle has a nominal charge of $+3$, and particles on the right each have a nominal charge of $+1$. Inset in (b) shows a triangular geometry of three body interaction, with the total surface charge density mapped out on each particle for the case of $k_1 = k_2 = k_3 = 20$ and $s = 0.2$.

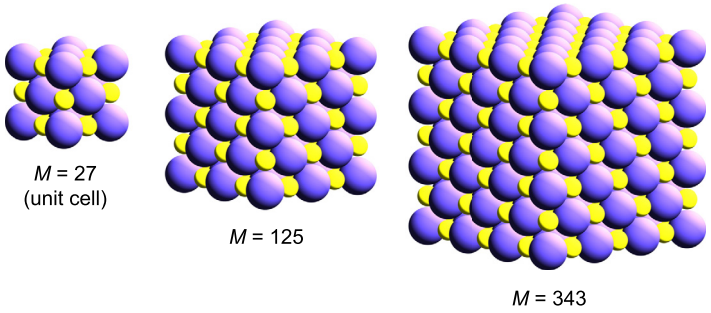

Fig. 11. Halite ('rock-salt') structure of sodium chloride (NaCl), where the sodium cation is depicted in yellow and chlorine anion in blue. Shown are the first three cubic structures starting with the unit cell.

to the square of the distance between interacting particles, for polarization terms there is a higher order inverse relation between separation and force.

3.6. Halite lattice and estimation of the Madelung constant

Sodium chloride (NaCl) occurs naturally in a (6,6)-coordinate halite ('rock-salt'), cubic structure, where each cation is surrounded by six anions and vice versa [53], as illustrated in Fig. 11. For a crystal, the lattice energy is defined as the difference in electrostatic potential energy between the salt packed in solid form and its isolated constituents, in this case Na^+ and Cl^-. If the constituents interact to form ion pairs instead of a lattice, then the energy released would be considerably smaller than that observed for the lattice energy. This difference is reflected in the Madelung constant, which is the ratio between the lattice energy per mol of a substance in a crystal form and the potential energy per mol of isolated ion pairs [54]. The knowledge of the Madelung constant for crystals is important as it can be used to estimate lattice energies directly by treating the crystal's constituents as point charges [55]. The Madelung constant also reflects the type of lattice structure present in a crystalline form.

The potential energy of a finite unit cell of a crystal is expected to differ from the lattice energy of the infinite bulk structure. Fig. 12 shows that as the number of atoms in the unit cell increases the potential energy of the unit cell approaches the value of the total lattice energy. The estimated lattice energy and Madelung constant for sodium chloride are plotted as a function of the number of particles M in the unit cell indicating that as M increases, the estimated lattice energy and Madelung constant asymptotically approach their reference values [56] of 750.619 kJ mol^{-1} and 1.74756, respectively.

4. Conclusions

A general solution to the problem of calculating many-body electrostatic interactions between collections of charged dielectric particles is presented. The model quantitatively and accurately describes the mutual polarization experienced by interacting particles, and it is particularly suitable for calculating electrostatic interactions in systems that strongly deviate from purely Coulombic behavior. Physically meaningful interpretation of electrostatic self-assembly and ordering of colloidal particles, formation of structurally diverse binary nanocrystal superlattices [58,20], crystallization of deformable objects, such

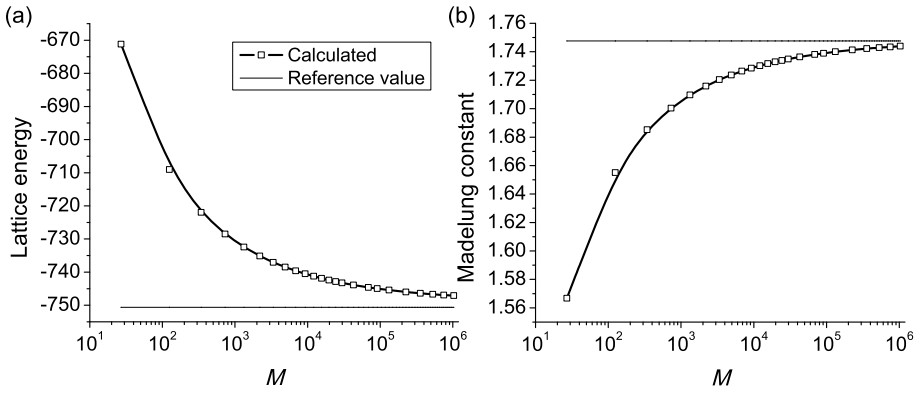

Fig. 12. Semi-log plot of the estimated lattice energy (a) and estimated Madelung constant (b), as function of the number of particles, M, in the structure. The sodium cation is represented by a sphere of radius 1.02 Å [56] carrying a positive elementary charge, and the chlorine anion is represented by a sphere of radius 1.81 Å [56] carrying a negative elementary charge. Unlike the previous calculations presented here, these results are not dimensionless, hence, the actual value of Coulomb's constant has been used. The lattice energy is presented as a Coulombic component added by the Born force component from Born–Landé equation, the latter being proportional to B/h^n, where B is a repulsion coefficient, h is the internuclear distance, and n is the Born exponent [57].

as micelles and globular proteins, that can adapt their structure to the local coordination environment, depends strongly on accurate description of many-body effects and non-pairwise interactions. Inclusion of many-body interactions, using the proposed model, will aid prediction and precise control of nanoparticle size, shape and composition, which generally affect electronic, optical and magnetic properties of the nanoparticle superlattice. Finer control of these properties is an important step towards the design of metamaterials with pre-defined physical characteristics.

Linear scaling of the presented many-body problem for the interaction energy with the number of particles in a system ensures fast and efficient computation and a good convergence of the solution up to the point where particles touch. A full linear scaling implementation of the forces is a more delicate task that we are focusing on in future.

The method turns out to be very efficient due to a direct interplay between surface density approximations on the spheres in terms of truncated spherical harmonics series and an equivalent multipolar distribution at the sphere's center. The method is based on a Galerkin approach and thus stands on a solid mathematical ground. Further, no error is committed in approximating the geometry since no meshing of the particles is required, which, in turn, allows also very efficient discretizations for polydisperse configurations. We also want to emphasize that the method is a high-order spectral method so that exponential convergence is achieved for smooth solutions which is the case in our context. Further, the variational setting allows to explore the self-adjointness of the single layer boundary operator and to finally compute the forces acting on the spheres also efficiently.

This makes it suitable for use as a force field in many-body classical particle dynamics. This capability of the model opens up new application areas related to classical dynamics simulations exploring the consequences of changing the charge and the dielectric constant of nanoparticles on electrostatic assembly in the absence of other external influences. Whitesides and co-workers have produced extensive observations of contact electrification to create two-dimensional model electrostatic self-assembly [18,19]. These observations are related to experiments on the assembly of polymer particles of varying size and composition that have been subjected to tribocharging to acquire a positive or negative charge. A consequence of the resultant electrostatic interactions is self-organization of the charged particles into a range of lattice structures. Our classical dynamics simulations [42], based on the proposed many-body solution, successfully reproduced many of the observed patterns of behavior. This study reveals the importance of taking many-body interactions into account, and the calculations also show how particle polarizability influences the assembly process.

Acknowledgements

EBL thanks the University of Nottingham, where he worked on part of his contributions to the manuscript. EB acknowledges the financial support of an ERC Consolidator grant (Project-ID 307755-FIN). AJS would like to thank the Leverhulme Trust for the award of an Emeritus Fellowship. BS acknowledges the funding from the German Academic Exchange Service (DAAD) from funds of the "Bundesministeriums für Bildung und Forschung" (BMBF) for the project Aa-Par-T (Project-ID 57317909). YM acknowledges the funding from the PICS-CNRS (Project N° 230509) as well as the PHC PROCOPE 2017 (Project N° 37855ZK) and part of this work has benefited from French state funding managed by CALSIMLAB and the ANR within the Investissements d'Avenir programme under reference ANR-11-IDEX-0004-02.

References

[1] B. Tinsley, The global atmospheric electric circuit and its effects on cloud microphysics, Rep. Prog. Phys. 71 (6) (2008) 066801, https://doi.org/10.1088/0034-4885/71/6/066801.

[2] T. Mather, R. Harrison, Electrification of volcanic plumes, Surv. Geophys. 27 (4) (2006) 387–432, https://doi.org/10.1007/s10712-006-9007-2.
[3] Y. Liang, N. Hilal, P. Langston, V. Starov, Interaction forces between colloidal particles in liquid: theory and experiment, Adv. Colloid Interface Sci. 134 (2007) 151–166, https://doi.org/10.1016/j.cis.2007.04.003.
[4] H. Ohshima, Electrostatic interaction between a sphere and a planar surface: generalization of point-charge/surface image interaction to particle/surface image interaction, J. Colloid Interface Sci. 198 (1) (1998) 42–52, https://doi.org/10.1006/jcis.1997.5240.
[5] E. Bichoutskaia, A.L. Boatwright, A. Khachatourian, A.J. Stace, Electrostatic analysis of the interactions between charged particles of dielectric materials, J. Chem. Phys. 133 (2010) 024105, https://doi.org/10.1063/1.3457157.
[6] H. Zettergren, B.O. Forsberg, H. Cederquist, Are single C_{60} fullerenes dielectric or metallic? Phys. Chem. Chem. Phys. 14 (47) (2012) 16360–16364, https://doi.org/10.1039/c2cp42884a.
[7] V. Munirov, A. Filippov, Interaction of two dielectric macroparticles, J. Exp. Theor. Phys. 117 (5) (2013) 809–819, https://doi.org/10.1134/S1063776113130050.
[8] T. Murovec, C. Brosseau, Electrostatics of two charged conducting ellipsoids, Appl. Phys. Lett. 102 (8) (2013) 084105, https://doi.org/10.1063/1.4793664.
[9] A. Khachatourian, H.-K. Chan, A.J. Stace, E. Bichoutskaia, Electrostatic force between a charged sphere and a planar surface: a general solution for dielectric materials, J. Chem. Phys. 140 (7) (2014) 074107, https://doi.org/10.1063/1.4862897.
[10] P. Linse, Electrostatics in the presence of spherical dielectric discontinuities, J. Chem. Phys. 128 (21) (2008) 214505, https://doi.org/10.1063/1.2908077.
[11] J. Lekner, Electrostatics of two charged conducting spheres, Proc. R. Soc. A 468 (2012) 2829–2848, https://doi.org/10.1098/rspa.2012.0133.
[12] A.J. Stace, A.L. Boatwright, A. Khachatourian, E. Bichoutskaia, Why like-charged particles of dielectric materials can be attracted to one another, J. Colloid Interface Sci. 354 (1) (2011) 417–420, https://doi.org/10.1016/j.jcis.2010.11.030.
[13] E.B. Lindgren, I.N. Derbenev, A. Khachatourian, H.-K. Chan, A.J. Stace, B.E., Electrostatic self-assembly: understanding the significance of the solvent, J. Chem. Theory Computat. 14 (2018) 905–915.
[14] E.B. Lindgren, B. Stamm, H.-K. Chan, Y. Maday, A.J. Stace, E. Besley, The effect of like-charge attraction on aerosol growth in the atmosphere of titan, Icarus 291 (2017) 245–253, https://doi.org/10.1016/j.icarus.2016.12.013.
[15] A.J. Stace, E. Bichoutskaia, Treating highly charged carbon and fullerene clusters as dielectric particles, Phys. Chem. Chem. Phys. 13 (41) (2011) 18339–18346, https://doi.org/10.1039/c1cp21573f.
[16] A. Stace, E. Bichoutskaia, Absolute electrostatic force between two charged particles in a low dielectric solvent, Soft Matter 8 (23) (2012) 6210–6213, https://doi.org/10.1039/c2sm25602a.
[17] M. Brunner, J. Dobnikar, H.-H. von Grünberg, C. Bechinger, Direct measurement of three-body interactions amongst charged colloids, Phys. Rev. Lett. 92 (7) (2004) 078301, https://doi.org/10.1103/PhysRevLett.92.078301.
[18] B.A. Grzybowski, A. Winkleman, J.A. Wiles, Y. Brumer, G.M. Whitesides, Electrostatic self-assembly of macroscopic crystals using contact electrification, Nat. Mater. 2 (4) (2003) 241–245, https://doi.org/10.1038/nmat860.
[19] L.S. McCarty, A. Winkleman, G.M. Whitesides, Electrostatic self-assembly of polystyrene microspheres by using chemically directed contact electrification, Angew. Chem., Int. Ed. Engl. 46 (1–2) (2007) 206–209, https://doi.org/10.1002/anie.200602914.
[20] E.V. Shevchenko, D.V. Talapin, N.A. Kotov, S. O'brien, C.B. Murray, Structural diversity in binary nanoparticle superlattices, Nature 439 (7072) (2006) 55–59, https://doi.org/10.1038/nature04414.
[21] R. Messina, Image charges in spherical geometry: application to colloidal systems, J. Chem. Phys. 117 (24) (2002) 11062–11074, https://doi.org/10.1063/1.1521935.
[22] Z. Xu, Electrostatic interaction in the presence of dielectric interfaces and polarization-induced like-charge attraction, Phys. Rev. E 87 (1) (2013) 013307, https://doi.org/10.1103/PhysRevE.87.013307.
[23] J. Qin, J. Li, V. Lee, H. Jaeger, J.J. de Pablo, K.F. Freed, A theory of interactions between polarizable dielectric spheres, J. Colloid Interface Sci. 469 (2016) 237–241, https://doi.org/10.1016/j.jcis.2016.02.033.
[24] P.T. Metzger, J.E. Lane, Electric potential due to a system of conducting spheres, J. Appl. Phys. 2 (2009) 32–48, https://doi.org/10.2174/1874183500902010032.
[25] H. Clercx, G. Bossis, Many-body electrostatic interactions in electrorheological fluids, Phys. Rev. E 48 (4) (1993) 2721, https://doi.org/10.1103/PhysRevE.48.2721.
[26] B. Kemp, J. Whitney, Electrostatic adhesion of multiple non-uniformly charged dielectric particles, J. Appl. Phys. 113 (4) (2013) 044903, https://doi.org/10.1063/1.4789014.
[27] H. Hoshi, M. Sakurai, Y. Inoue, R. Chûjô, Medium effects on the molecular electronic structure. I. the formulation of a theory for the estimation of a molecular electronic structure surrounded by an anisotropic medium, J. Chem. Phys. 87 (2) (1987) 1107–1115.
[28] R. Bharadwaj, A. Windemuth, S. Sridharan, B. Honig, A. Nicholls, The fast multipole boundary element method for molecular electrostatics: an optimal approach for large systems, J. Comput. Chem. 16 (7) (1995) 898–913.
[29] K. Barros, D. Sinkovits, E. Luijten, Efficient and accurate simulation of dynamic dielectric objects, J. Chem. Phys. 140 (6) (2014) 064903.
[30] P. Cazeaux, O. Zahm, A fast boundary element method for the solution of periodic many-inclusion problems via hierarchical matrix techniques, ESAIM Proc. Surv. 48 (2015) 156–168.
[31] D. McKenzie, R. McPhedran, G. Derrick, The conductivity of lattices of spheres—II. The body centred and face centred cubic lattices, Proc. R. Soc. Lond. A 362 (1978) 211–232.
[32] R. McPhedran, D. McKenzie, The conductivity of lattices of spheres I. The simple cubic lattice, Proc. R. Soc. Lond. A 359 (1978) 45–63.
[33] A. Sangani, A. Acrivos, The effective conductivity of a periodic array of spheres, Proc. R. Soc. Lond. A 386 (1983) 263–275.
[34] K. Hinsen, B. Felderhof, Dielectric constant of a suspension of uniform spheres, Phys. Rev. B 46 (20) (1992) 12955.
[35] L. Greengard, M. Moura, On the numerical evaluation of electrostatic fields in composite materials, Acta Numer. 3 (1994) 379–410.
[36] Z. Gan, S. Jiang, E. Luijten, Z. Xu, A hybrid method for systems of closely spaced dielectric spheres and ions, SIAM J. Sci. Comput. 38 (3) (2016) B375–B395.
[37] J. Lai, M. Kobayashi, L. Greengard, A fast solver for multi-particle scattering in a layered medium, Opt. Express 22 (17) (2014) 20481–20499.
[38] J. Lai, M. Kobayashi, A. Barnett, A fast and robust solver for the scattering from a layered periodic structure containing multi-particle inclusions, J. Comput. Phys. 298 (2015) 194–208.
[39] Z. Gimbutas, L. Greengard, Fast multi-particle scattering: a hybrid solver for the Maxwell equations in microstructured materials, J. Comput. Phys. 232 (1) (2013) 22–32.
[40] M. Ganesh, S.C. Hawkins, R. Hiptmair, Convergence analysis with parameter estimates for a reduced basis acoustic scattering t-matrix method, IMA J. Numer. Anal. 32 (4) (2012) 1348–1374, https://doi.org/10.1093/imanum/drr041.
[41] M. Ganesh, S. Hawkins, An efficient $\mathcal{O}(N)$ algorithm for computing $\mathcal{O}(N^2)$ acoustic wave interactions in large N-obstacle three dimensional configurations, BIT Numer. Math. 55 (1) (2015) 117–139.
[42] E.B. Lindgren, B. Stamm, Y. Maday, E. Besley, A.J. Stace, Dynamic simulations of many-body electrostatic self-assembly, Philos. Trans. R. Soc. 376 (2115) (2018) 5936–5949.
[43] S.A. Sauter, C. Schwab, Boundary element methods, in: Boundary Element Methods, Springer, 2010, pp. 183–287.
[44] V. Lebedev, D. Laikov, A quadrature formula for the sphere of the 131st algebraic order of accuracy, in: Doklady. Mathematics, vol. 59, MAIK Nauka/Interperiodica, 1999, pp. 477–481.

[45] E. Cancès, Y. Maday, B. Stamm, Domain decomposition for implicit solvation models, J. Chem. Phys. 139 (5) (2013) 054111.
[46] B. Stamm, E. Cancès, F. Lipparini, Y. Maday, A new discretization for the polarizable continuum model within the domain decomposition paradigm, J. Chem. Phys. 144 (5) (2016) 054101.
[47] V. Rokhlin, Rapid solution of integral equations of classical potential theory, J. Comput. Phys. 60 (2) (1985) 187–207.
[48] L. Greengard, V. Rokhlin, A fast algorithm for particle simulations, J. Comput. Phys. 73 (2) (1987) 325–348.
[49] P. Blanchard, B. Bramas, O. Coulaud, E. Darve, L. Dupuy, A. Etcheverry, G. Sylvand, Scalfmm: a generic parallel fast multipole library, in: Computational Science and Engineering (CSE), 2015.
[50] P. Fortin, High Performance Parallel Hierarchical Algorithmic for N-Body Problems, Theses, Université Sciences et Technologies - Bordeaux I, Nov. 2006, https://tel.archives-ouvertes.fr/tel-00135843.
[51] E.B. Lindgren, H.-K. Chan, A.J. Stace, E. Besley, Progress in the theory of electrostatic interactions between charged particles, Phys. Chem. Chem. Phys. 18 (8) (2016) 5883–5895, https://doi.org/10.1039/c5cp07709e.
[52] A.J. Stone, The Theory of Intermolecular Forces, 2nd edition, Oxford University Press, Oxford, 2013.
[53] P. Atkins, J. de Paula, Atkins' Physical Chemistry, 9th edition, W. H. Freeman, 2010.
[54] J.E. House, Inorganic Chemistry, 2nd edition, Academic Press, 2013.
[55] E. Bichoutskaia, N.C. Pyper, Fundamental global model for the structures and energetics of nanocrystalline ionic solids, J. Phys. Chem. B 110 (12) (2006) 5936–5949, https://doi.org/10.1021/jp055800g.
[56] W.M. Haynes (Ed.), CRC Handbook of Chemistry and Physics, 97th edition, CRC Press, 2016.
[57] C.E. Housecroft, A.G. Sharpe, Inorganic Chemistry, 2nd edition, Pearson, 2005.
[58] M.A. Boles, D.V. Talapin, Many-body effects in nanocrystal superlattices: departure from sphere packing explains stability of binary phases, J. Am. Chem. Soc. 137 (2015) 4494–4502, https://doi.org/10.1021/jacs.5b00839.